SUPPLEMENTARY MATERIAL

Synthesis, characterization, antimicrobial and cytotoxic activity and DNA binding properties of d-metal complexes with hydrazones of Girard's T and P reagents

Nevena Stevanović,[1] Paolo Pio Mazzeo,[2,3] Alessia Bacchi,[2,3] Ivana Z. Matić,[4] Marija Đorđić Crnogorac,[4] Tatjana Stanojković,[4] Miroslava Vujčić,[5] Irena Novaković,[5] Dušanka Radanović,[5] Maja Šumar-Ristović,[1] Dušan Sladić,[1] Božidar Čobeljić,[1] Katarina Anđelković[1,*]

[1]University of Belgrade-Faculty of Chemistry, Studentski trg 12–16, 11000 Belgrade, Serbia

[2]Dipartimento di Scienze Chimiche, della Vita e della Sostenibilità Ambientale, Università degli Studi di Parma, Viale delle Scienze, 17A, 43124 Parma, Italy

[3]Biopharmanet-TEC, Università Degli Studi di Parma, via Parco Area delle Scienze 27/A, Parma, 43124, Italy

[4]Institute of Oncology and Radiology of Serbia, 11000 Belgrade, Serbia

[5]University of Belgrade-Institute of Chemistry, Technology and Metallurgy, Department of Chemistry, Njegoševa 12, 11000 Belgrade, Serbia

Contents

* Corresponding author.

E-mail address: kka@chem.bg.ac.rs (K. Anđelković)

Synthesis and characterization

Synthesis of ligand **HL^3**Cl

The ligand **HL^3**Cl was synthesized by the reaction of 2-acetylpyridine and Girard's T reagent in methanol according to the previously described method [1]. IR (ATR, cm^{-1}): 3384 (w), 3123 (m), 3095 (m), 3054 (m), 2952 (s), 1704 (vs), 1551 (s), 1485 (m), 1400 (m), 1300 (w), 1253 (w), 1200 (s), 1153 (w), 1135 (m), 1095 (w), 944 (w), 914 (m), 683 (w). Elemental analysis calcd. for $C_{12}H_{19}N_4OCl$: C 53.23%, H 7.07%, N 20.69%; found: C 53.15%, H 7.10%, N 20.59%.

Synthesis of complex **3** ([Zn**L^2**$(NCS)_2$]×$2H_2O$)

The Zn(II) complex **3** was synthesized by the reaction of ligand **HL^2**Cl, $Zn(OAc)_2$×$2H_2O$ and NH_4SCN according to the previously described method [2]. IR (ATR, ATR, cm^{-1}): 3502 (s), 3383 (s), 3124 (m), 2959 (w), 2088 (vs), 1612 (s), 1534 (s), 1475 (s), 1424 (s), 1405 (s), 1341 (m), 1290 (w), 1151 (w), 1068 (w), 990 (w), 876 (w), 747 (w). Elemental analysis calcd. for $C_{12}H_{20}ZnN_6O_3S_3$: C 36.71%, H 5.13%, N 21.41%, S 24.51%; found: C 36.73%, H 5.10%, N 21.45%, S 24.39%. λ_M = 13.2 $\Omega^{-1}cm^2mol^{-1}$.

Synthesis of complex **4** $[Ni_2$**L^2**$_2(\mu\text{-}_{1,1}\text{-}N_3)_2(N_3)_2]$×$4H_2O$

The Cu(II) complex **4** was synthesized by the reaction of ligand **HL^2**Cl, $NiCl_2$×$6H_2O$ and NaN_3 according to the previously described method [3]. IR (ATR, ATR, cm^{-1}): 3395 (m), 3096 (w), 2148 (m), 2053 (vs), 2034 (vs), 1531 (s), 1480 (m), 1404 (m), 1247 (m), 1012 (m), 975 (w), 913 (w), 888 (w), 736 (w), 641 (w). Elemental analysis calcd. for $C_{20}H_{40}N_{20}Ni_2O_6S_2$: C 28.66%, H 4.81%, N 33.42%; found: C 28.59%, H 4.88%, N 33.38%. λ_M = 15.4 $\Omega^{-1}cm^2mol^{-1}$.

Synthesis of complex **5** ([Zn**L^3**$(NCS)_2$]×0.5MeOH)

The Zn(II) complex **5** was synthesized by the reaction of ligand **HL^3**Cl, $Zn(OAc)_2$×$2H_2O$ and NH_4SCN according to the previously described method [1]. IR (ATR, ATR, cm^{-1}): 3033 (w), 2065 (vs), 1639 (w), 1595 (w), 1564 (m), 1535 (s), 1461 (m), 1434 (m), 1395 (m), 1364 (m), 1339 (m), 1302 (m), 1200 (w), 1145 (w), 1074 (m), 1019 (m), 966 (w) 914 (w), 749 (w). Elemental analysis calcd. for $C_{14.5}H_{20}N_6O_{1.5}S_2Zn$: C 38.75%, H 4.65%, N 19.37%, S 14.78%; found: C 38.71%, H 4.68%, N 20.05%, S 19.29%. λ_M = 13.8 $\Omega^{-1}cm^2mol^{-1}$.

Synthesis of complex **6** ($[Cu_2$**L^3**$_2(\mu\text{-}_{1,1}\text{-}N_3)_2](ClO_4)_2$)

The Cu(II) complex **6** was synthesized by the reaction of ligand **HL^3**Cl and $Cu(ClO_4)_2$×$6H_2O$ excess of NaN_3 according to the previously described method [4]. IR (ATR, ATR, cm^{-1}): 3520 (m), 3350 (m), 2040 (vs), 1628 (w), 1567 (w), 1524 (m), 1468 (w), 1339 (m), 1297 (m), 1146 (w), 1078

(w), 1027 (w), 910 (w), 779 (w), 684 (w). Elemental analysis calcd. for $C_{24}H_{36}Cl_2Cu_2N_{14}O_{10}$: C 32.81%, H 4.13%, N 22.32%; found: C 32.79%, H 4.18%, N 22.18%. λ_M = 30.6 $\Omega^{-1}cm^2mol^{-1}$.

Synthesis of complex **7** ([Cd**HL**^{3}$(NCS)_3$])

The Cd(II) complex **7** was synthesized by the reaction of ligand **HL**^{3}Cl, $Cd(NO_3)_2\times4H_2O$ and NH_4SCN according to the previously described method [1]. IR (ATR, ATR, cm^{-1}): 3020 (w), 2092 (vs), 2048 (vs), 1683 (s), 1637 (w), 1592 (w), 1550 (m), 1474 (m), 1436 (w), 1327 (w), 1254 (w), 1227 (w), 1199 (w), 1155 (w), 1127 (w), 1101 (w), 966 (w), 929 (w), 779 (w). Elemental analysis calcd. for $C_{15}H_{19}CdN_7OS_3$: C 34.52%, H 3.67%, N 18.78%, S 18.43%; found: C 34.47%, H 3.68%, N 18.72%, S 18.39%. λ_M = 16.9 $\Omega^{-1}cm^2mol^{-1}$.

Synthesis of complex **8** ([Cu**L**^{3}Cl](ClO_4))

The Cu(II) complex **8** was synthesized by the reaction of ligand **HL**^{3}Cl and $Cu(ClO_4)_2\times6H_2O$ according to the previously described method [4]. IR (ATR, ATR, cm^{-1}): 3096 (w), 3037 (w), 1603 (w), 1573 (w), 1525 (s), 1473 (m), 1447 (s), 1400 (m), 1374 (w), 1339 (m), 1316 (w), 1263 (w), 1152 (w), 1075 (vs), 966 (w), 930 (w), 912 (m), 785 (m), 682 (w), 625 (m), 568 (w). Elemental analysis calcd. for $C_{12}H_{18}Cl_2CuN_4O_5$: C 33.31%, H 4.19%, N 12.95.%; found: C 33.29%, H 4.20%, N 12.91%. λ_M = 22.1 $\Omega^{-1}cm^2mol^{-1}$.

Synthesis of complex **9** ([Cu**L**^{3}Cl](NO_3))

The Cu(II) complex **9** was synthesized by the reaction of ligand **HL**^{3}Cl and $Cu(NO_3)_2\times3H_2O$ according to the previously described method [5]. IR (ATR, ATR, cm^{-1}): 3373 (vs), 3271 (vs), 3059 (m), 3031 (m), 1595 (vs), 1561 (m), 1529 (w), 1482 (s), 1443 (s), 1365 (m), 1307 (m), 1265 (w), 1196 (w), 1167 (m), 1118 (w), 1074 (w), 1048 (w), 1021 (w), 784 (s), 675 (w), 575 (w).. Elemental analysis calcd. for $C_{12}H_{18}ClCuN_5O_4$: C 36.46%, H 4.59%, N 17.72%; found: C 36.41%, H 4.60%, N 17.75%. λ_M = 21.8 $\Omega^{-1}cm^2mol^{-1}$.

Synthesis of complex **10** ([Co**L**$^3{}_2$][$Co(NCS)_4$]BF_4)

The Co(III) complex **10** was synthesized by the reaction of ligand **HL**^{3}Cl, $Co(BF_4)_2\times6H_2O$ and NH_4SCN according to the previously described method [6]. IR (ATR, ATR, cm^{-1}): 3080 (w), 2065 (vs), 1625 (w), 1601 (w), 1519 (s), 1466 (m), 1397 (m), 1375 (m), 1310 (m), 1264 (w), 1236 (w), 1206 (w), 1152 (w), 1053 (s), 972 (w), 923(w), 766 (w). Elemental analysis calcd. for $C_{28}H_{36}BCo_2F_4N_{12}O_2S_4$: C 37.14%, H 4.01%, N 18.56%, S 14.16%; found: C 36.11%, H 4.10%, N 18.45%, S 14.39%. λ_M = 28.2 $\Omega^{-1}cm^2mol^{-1}$.

Synthesis of complex **11** ($[Ni_2\mathbf{L^3}_2(\mu\text{-}_{1,1}\text{-}N_3)_2(N_3)_2]\times 6H_2O$)

The Cu(II) complex **11** was synthesized by the reaction of ligand $\mathbf{HL^3}$Cl, $Ni(BF_4)_2\times 6H_2O$ and NaN_3 according to the previously described method [7]. IR (ATR, ATR, cm^{-1}): 3345 (s), 3037 (w), 2040 (vs), 1619 (w), 1595 (w), 1540 (s), 1469 (m), 1300 (m), 1245 (w), 1145 (w), 1023 (w), 973 (w), 781 (w), 676 (w), 571 (w). Elemental analysis calcd. for $C_{24}H_{48}N_{20}Ni_2O_8$: C 33.43%, H 5.61%, N 32.49 %; found: C 33.39%, H 5.68%, N 32.38%. λ_M = 15.7 $\Omega^{-1}cm^2mol^{-1}$.

Synthesis of complex **12** ($[Fe\mathbf{L^3}(NCS)_3]$)

The Fe(III) complex **12** was synthesized by the reaction of ligand $\mathbf{HL^3}$Cl, $Fe(NO_3)_3\times 9H_2O$ and NH_4SCN according to the previously described method [8]. IR (ATR, ATR, cm^{-1}): 3074 (w), 2036 (s), 2027 (s), 1620 (m), 1598 (m), 1566 (m), 1463 (m), 1392 (m), 1261 (w), 1166 (w), 1144 (w), 1113 (w), 1025 (w), 968 (w), 906 (w), 806 (w), 675 (w). Elemental analysis calcd. for $C_{12}H_{20}ZnN_6O_3S_3$: C 36.71%, H 5.13%, N 21.41%, S 24.51%; found: C 36.73%, H 5.10%, N 21.45%, S 24.39%. λ_M = 12.2 $\Omega^{-1}cm^2mol^{-1}$.

Spectroscopic characterization of complexes 1 and 2

IR spectra

On the basis of IR spectroscopy results for complex **1**, coordination of $\mathbf{HL^1}$Cl ligand in deprotonated *α*-oxyazine form was confirmed. The new band at 1518 cm^{-1} in the spectrum of Zn(II) complex, corresponding to ν($^-$O–C=N) vibration of deprotonated hydrazide moiety, appeared instead of the band of carbonyl group of non-coordinated hydrazide of $\mathbf{HL^1}$Cl at 1695 cm^{-1}. In the IR spectrum of Zn(II) complex a strong band at 2075 cm^{-1} can be attributed to the vibration of coordinated thiocyanate ions.

In the spectrum of complex **2**, band corresponding to vibration of coordinated carbonyl group appeared at 1656 cm^{-1} instead of the bond of non-coordinated form of $\mathbf{HL^2}$Cl at 1701 cm^{-1}. Coordination of azomethine nitrogen atom resulted in bathochromic shift of ν(C=N) vibration from 1550 cm^{-1} in the spectrum of $\mathbf{HL^2}$Cl to 1529 cm^{-1} in the spectrum of Bi(III) complex. Coordination of thiazole nitrogen atom resulted in shift of the bond at 1486 cm^{-1} in the spectrum of $\mathbf{HL^2}$Cl to 1475 cm^{-1} in the spectrum of Bi(III) complex.

NMR (^{1}H and ^{13}C) spectra

The signal of hydrazide NH is absent in the ^{1}H NMR spectra of complex **1** indicating that the ligand is coordinated in deprotonated zwitter-ionic form. Coordination of azomethine nitrogen in Zn(II) complex can be confirmed from downfield shift of C9-H from 8.32 ppm in the spectrum of $\mathbf{HL^1}$Cl to 8.56 ppm in the spectrum of Zn(II) complex. Due to coordination of carbonyl oxygen atom,

signal of the carbonyl carbon (C10) is shifted downfield from 167.43 ppm in the spectrum of **HL[1]**Cl to 175.20 ppm in the spectra of complex. Upfield shift of azomethine carbon atom (C9) signal from 146.05 ppm in the spectrum of **HL[1]**Cl to 144.00 ppm in the spectrum of Zn(II) complex indicates coordination of azomethine nitrogen. Coordination of quinoline nitrogen atom caused upfield shift of C2 atom signal from 153.33 ppm in the spectrum of **HL[1]**Cl to 149.41 ppm in the spectra of Zn(II) complex. In the ^{13}C NMR spectrum of Zn(II) complex the signal of coordinated SCN^- ion was observed at 134.73 ppm.

Complex **2** is not stable in DMSO solution. Appearance of series of signals in ^{1}H NMR spectrum of Bi(III) complex in DMSO-d_6 solution indicates its instability and replacement of coordinated **HL[2]**Cl ligand by DMSO. A similar replacement occurs in D_2O and methanol-d_4, while in solvents with lower polarity Bi(III) complex was not soluble.

UV-Vis spectra and molar conductivity

The stability of complexes used for the biological study **1**, **3**–**12** was investigated by UV-Vis spectroscopy and molar conductivity measurements in the freshly prepared DMSO solutions (Fig. S3). For complex **1** additional UV-Vis absorption spectra were recorded after 24 h. For all previously synthesized complexes, **3**–**12**, data gathered by UV-Vis and molar conductivity showed agreement between structures in the solid and solution thus indicating their stability in solution. In the case of complex **1** no significant spectral shifts were observed upon comparing spectra of freshly prepared solution, and solution which was left overnight (Fig. S4). The low value of molar conductivity for complex **1** indicates nonelectrolyte type of solution which supports conclusions obtained from NMR and UV-Vis spectroscopy that no structural changes occurred in solution.

Brine shrimp assay and DPPH radical scavenging activity

About 20 g of commercially purchased lyophilized eggs of *Artemia salina* was added to 0.5 L of tap water, and air was passed through the suspension by pump under illumination for 48 h. All tested compounds were dissolved in DMSO and various amounts (0.01–1 mg) were added to 950 μL of artificial seawater with freshly hatched nauplii. After 24 h illumination at room temperature, the number of dead and surviving nauplii were counted and statistically analyzed. LC_{50} was defined as a concentration of compounds that caused the death of 50% of the nauplii. All samples were done in triplicate.

The 2,2-diphenyl-1-picrylhydrazyl (DPPH) radical scavenging activity was determined by the method of Blois.[9] Commercially available free radical DPPH was dissolved in methanol at concentration of 6.58×10^{-5} M, while tested compounds were dissolved in DMSO. Into a 96-well

microplate, 50 μL solutions of the tested compounds at concentrations range 10 to 0.02 mg/mL were loaded (50 μL DMSO in the control), and 100 μL of DPPH solution were added. After incubation for 30 min at room temperature in the dark, the absorbance was measured at 517 nm. All the measurements were performed in triplicate and the scavenging activity of the tested derivatives was calculated as:

$$\text{Scavenging activity (\%)} = 100 \times (A_{\text{control}} - (A_{\text{sample}} - A_0)) / A_{\text{control}}$$

where A_{control} and A_{sample} refer to the absorbance of DPPH in control solution and sample, respectively, while A_0 refers to the absorbance of the solutions of compounds, because of their colour.

The IC_{50} was defined as the antioxidant concentration necessary to decrease the amount of the initial DPPH radical by 50 % and was calculated from the plotted graph of scavenging activities against the concentrations of the tested compounds. Ascorbic acid was employed as the positive control (concentrations from 50 to 500 μg mL^{-1}).

The results of toxicity of complexes and their precursors against nauplii of the *Artemia salina* as well as radical scavenging activity are given at Table S3. Neither of the tested ligands showed toxicity, while the salts $Cu(ClO_4)_2 \times 6H_2O$ and $Cu(NO_3)_2 \times 3H_2O$ showed the highest toxicity of the tested salts. All tested complexes showed generally low toxicity, except **1** the toxicity of which was twice lower than control compound $K_2Cr_2O_7$. This result is not surprising. Since nauplii of the *Artemia salina* live in symbiosis with some types of bacteria and this complex displayed the strongest antibacterial activity, the toxicity may be due to the destruction of symbiotic bacteria.

The DPPH test showed that the ability of the two complexes **10** and **12** to scavenge radicals is almost four times higher than ascorbic acid. It is likely that the mode of complexation of the bidentate ligand via nitrogen leaves sulfur free to exert the antioxidative activity.

Interaction with BSA

For BSA fluorescence measurements, BSA concentration in 40 mM bicarbonate buffer was kept constant in all samples, while the concentrations of the compounds were varied: in 1 mL of buffer 5 μL of stock solution of BSA (3 mg/mL) and 2.5 μL of stock solution of the compound were added and incubated for 30 min after which emission spectra in the range 295 to 500 nm were recorded (excitation wavelength 280 nm). Another 2.5 μL of the solution of complexes were successively added so that final concentrations of 1.25, 2.5, 3.75, 5, 6.25, 7.5 and 8.75×10^{-5} M were attained for **HL^1**Cl and **HL^3**Cl, and 5×10^{-6} M, 1, 1.5, 2, 2.5. 3 and 3.5×10^{-5} M for **1** and **12**. The change in the fluorescence intensity was measured.

Bovine serum albumin is the major soluble protein of circulary system and it has many physiological functions, primarily in the transport of many endogenous and exogenous ligands. [10] BSA has often been used as a model protein to measure the albumin-binding ability of drugs and metal complexes. The emission spectra of BSA in the absence and presence of the increasing concentrations of compounds **HL^3**Cl, **12**, **HL^1**Cl and **1** are shown in Fig. S9, a,b,c and d, respectively. In absence of a compound, a strong emission band at 335 nm was observed due to fluorescence of trypthophan residues. When a BSA was titrated with ligand **HL^3**Cl and complex **12**, similar spectral pattern was observed, however the decrease in fluorescence intensity at maximum wavelength was by 64% and by 85%, respectively. In case of ligand **HL^1**Cl the fluorescence intensity reduction reached 85% at 335 nm with generation of new band at 372.5 nm, while complex **1** reduced the fluorescence intensity by 88%. These results indicated the binding of all of the compounds to BSA. The obtained strong decrease in fluorescence intensity suggested that the compounds interacted with tryphtophan residue present in the hydrophobic cavity of the protein probably via noncordianated hydrophobic parts of ligand moiety and/or cation–π interactions. It could also be concluded that neither iron nor zinc as the central metal ion affected the interaction with BSA significatly. The fluorescence quenching data were further analyzed with the Stern-Volmer equation (3) as follows [11].

$$I_0/I = 1 + K_q\tau_0[Q] = 1 + K_{sv}[Q] \qquad (3)$$

$$K_q = K_{sv} / \tau_0 \qquad (4)$$

Where I and I_0 are the steady state fluorescence intensities in presence and absence of a quencher, respectively. K_{sv} is Stern-Volmer constant and [Q] is concentration of quencher; τ_0 is the average lifetime of the protein without the quencher. As shown in insets in Fig. S9a–d, K_{sv} for compounds **HL^3**Cl, **12**, **HL^1**Cl and **1** were calculated from the plot I_0/I versus [compound] as 1.18×10^{-4} M, 5.02×10^{-4} M, 12.12×10^{-4} M and 15.52×10^{-4} M, respectively. Taking average lifetime of the biomolecule is around 10^{-8} Ms^{-1} [12] K_q values for **HL^3**Cl, **12**, **HL^1**Cl and **1** were calculated as 1.18×10^{-12} M, 5.02×10^{-12} M, 12.12×10^{-12} M and 15.52×10^{-12} M, respectively indicating static quenching constant, i.e. a nonfluorescent complex formation occurs between the compound and BSA.

During static quenching process, relation between the fluorescence intensity and concentration of a quencher can be described as in Eq (5) [11]

$$\log [(I_0 - I)/I] = \log K_b + n\log[Q] \qquad (5),$$

where K_b denotes the degree of interaction of protein with quencher and n is the number of bidning sites. The values of K_b have been derived from the plots of log $[(I_0 - I)/I]$ *versus* log [compound] for **HL^3**Cl, **12**, **HL^1**Cl and **1** (Fig. S10a–d) and were calculated as 0.249, 0.232, 0.205 and 0.199,

respectively. The obtained results confirmed the previous conslusion that that a hydrophobic interaction takes place between BSA and the compound.

Table S1. Crystal data and structure refinement for complexes **1** and **2**

Identification code	**1**	**2**
Empirical formula	$C_{19}H_{14}N_6OS_2Zn$	$C_{10.5}H_{19}BiCl_4N_4O_{1.5}S$
Formula weight	471.85	608.14
Temperature/K	300.5	300.5
Crystal system	triclinic	monoclinic
Space group	P-1	C2/c
a/Å	8.421(1)	14.106(1)
b/Å	14.288(2)	9.3130(6)
c/Å	17.258(3)	30.379(2)
α/°	91.238(4)	90
β/°	97.966(4)	106.114(2)
γ/°	91.943(4)	90
Volume/Å^3	2054.4(6)	3834.1(5)
Z	4	8
ρ_{calc}g/cm^3	1.526	2.107
μ/mm^{-1}	1.422	9.870
F(000)	960.0	2312.0
Crystal size/mm^3	0.10 × 0.10 × 0.09	0.07 × 0.07 × 0.06
Radiation /Å	MoKα (λ = 0.71073)	MoKα (λ = 0.71073)
2Θ range for data collection/°	4.768 to 51.532	5.272 to 56.058
Index ranges	–10 ≤ h ≤ 10, –17 ≤ k ≤ 17, –21 ≤ l ≤ 21	–18 ≤ h ≤ 18, –12 ≤ k ≤ 12, –37 ≤ l ≤ 40
Reflections collected	34725	23905
Independent reflections	7813 [R_{int} = 0.0392, R_{sigma} = 0.0389]	4633 [R_{int} = 0.0533, R_{sigma} = 0.0461]
Data/restraints/parameters	7813/0/523	4633/13/213
Goodness-of-fit on F^2	1.044	1.106
Final *R* indexes [I>=2σ (I)]	R_1 = 0.0407, wR_2 = 0.1060	R_1 = 0.0366, wR_2 = 0.0611
Final *R* indexes [all data]	R_1 = 0.0614, wR_2 = 0.1226	R_1 = 0.0602, wR_2 = 0.0670
Largest ΔF max/min / e Å^{-3}	0.59/–0.42	0.97/–1.05

Table S2. Comparison of the metal coordination geometry of the two independent molecules in **1**

		Length/Å			**Length/Å**
Zn^1	O^1	2.190(3)	Zn^2	O^2	2.201(2)
Zn^1	N^1	2.224(3)	Zn^2	N^7	2.255(2)
Zn^1	N^2	2.043(3)	Zn^2	N^8	2.039(3)
Zn^1	N^5	1.980(3)	Zn^2	N^{11}	1.955(3)
Zn^1	N^6	1.955(3)	Zn^2	N^{12}	1.979(3)

			Angle/°				**Angle/°**
O^1	Zn^1	N^1	150.03(10)	O^2	Zn^2	N^7	148.36(9)

N^{2}	Zn^{1}	O^{1}	73.95(10)	N^{8}	Zn^{2}	O^{2}	73.49(10)
N^{2}	Zn^{1}	N^{1}	76.13(10)	N^{8}	Zn^{2}	N^{7}	75.75(10)
N^{5}	Zn^{1}	O^{1}	95.54(12)	N^{11}	Zn^{2}	O^{2}	99.54(12)
N^{5}	Zn^{1}	N^{1}	102.00(11)	N^{11}	Zn^{2}	N^{7}	103.52(12)
N^{5}	Zn^{1}	N^{2}	122.86(12)	N^{11}	Zn^{2}	N^{8}	123.65(12)
N^{6}	Zn^{1}	O^{1}	95.08(13)	N^{11}	Zn^{2}	N^{12}	105.43(14)
N^{6}	Zn^{1}	N^{1}	102.20(12)	N^{12}	Zn^{2}	O^{2}	96.13(11)
N^{6}	Zn^{1}	N^{2}	128.51(13)	N^{12}	Zn^{2}	N^{7}	98.27(11)
N^{6}	Zn^{1}	N^{5}	108.01(13)	N^{12}	Zn^{2}	N^{8}	130.74(13)
C^{11}	O^{1}	Zn^{1}	109.6(2)	C^{28}	O^{2}	Zn^{2}	109.1(2)
C^{1}	N^{1}	Zn^{1}	111.3(2)	C^{18}	N^{7}	Zn^{2}	110.9(2)
C^{5}	N^{1}	Zn^{1}	129.4(2)	C^{22}	N^{7}	Zn^{2}	129.8(2)
N^{3}	N^{2}	Zn^{1}	120.10(19)	N^{9}	N^{8}	Zn^{2}	120.4(2)
C^{10}	N^{2}	Zn^{1}	119.2(2)	C^{27}	N^{8}	Zn^{2}	119.3(2)
C^{35}	N^{5}	Zn^{1}	169.7(3)	C^{37}	N^{11}	Zn^{2}	167.5(3)
C^{36}	N^{6}	Zn^{1}	174.7(3)	C^{38}	N^{12}	Zn^{2}	154.6(3)

Table S3. Brine shrimp assay and DPPH radical scavenging activity.

	LD50 (mM)	DPPH (mM)
HL^{1}Cl	1.57±0.14	/
1	0.19±0.03	0.90±0.08
HL^{2}Cl	1.14±0.11	0.49±0.06
2	1.14±0.10	7.29±0.20
3	1.27±0.14	/
4	0.86±0.04	/
HL^{3}Cl	1.02±0.10	/
5	0.98±0.09	/
6	0.46±0.04	1.53±0.08
7	0.53±0.04	0.50±0.06
8	1.04±0.07	/
9	1.54±0.10	7.14±0.11
10	0.65±0.07	0.02±0.01
11	0.82±0.06	7.72±0.13
12	0.49±0.03	0.02±0.01
NH_4SCN	0.98±0.06	/
NaN_3	0.54±0.05	/
$Zn(BF_4)_2\times6H_2O$	0.88±0.07	/
$Zn(OAc)_2\times2H_2O$	1.18±0.10	/
$Ni(BF_4)_2\times6H_2O$	0.64±0.05	/
$Cd(NO_3)_2\times4H_2O$	0.50±0.02	/
$Fe(NO_3)_3\times9H_2O$	1.24±0.09	/
$Co(BF_4)_2\times6H_2O$	1.51±0.07	/
$Cu(ClO_4)_2\times6H_2O$	0.28±0.02	/
$Cu(NO_3)_2\times3H_2O$	0.24±0.02	/
$BiCl_3$	ND	ND
$K_2Cr_2O_7$	0.077±0.016	
Ascorbic acid	/	0.079±0.018

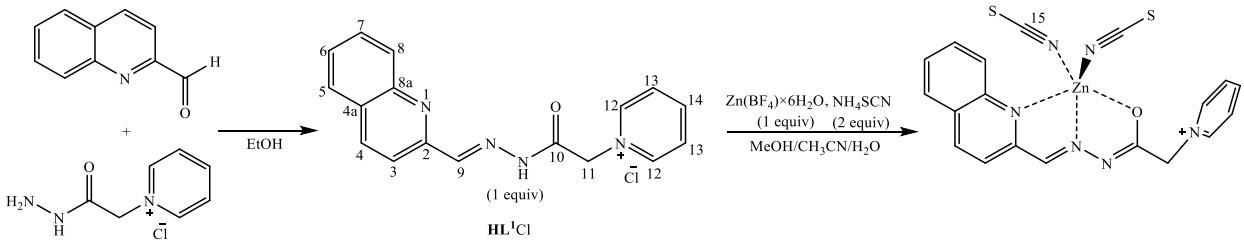

Scheme S1. Synthesis of the **HL[1]**Cl ligand and Zn(II) complex (**1**).

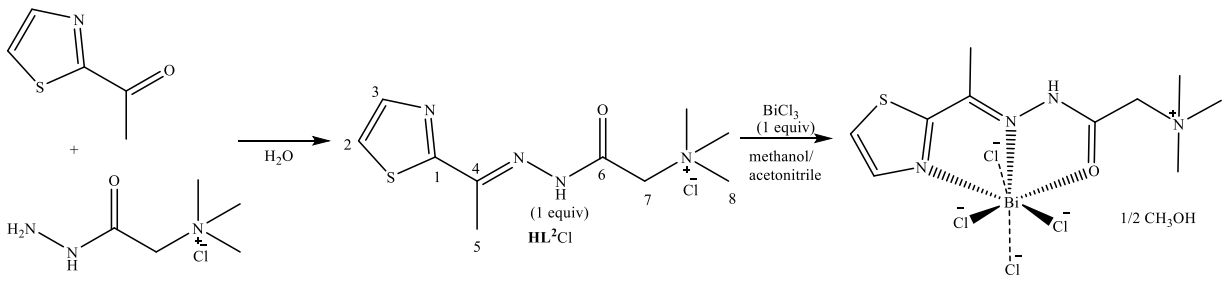

Scheme S2. Synthesis of the **HL[2]**Cl ligand and Bi(III) complex (**2**).

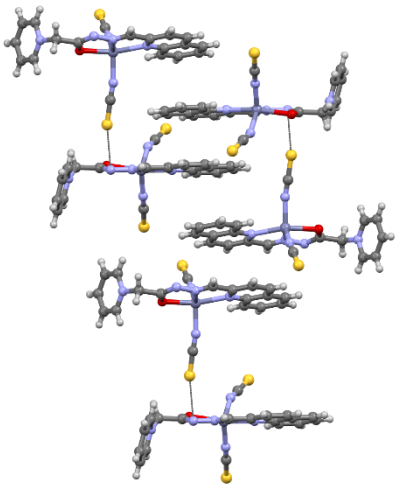

Fig. S1 Packing arrangement of **1**, displaying a chalcogen bond (dotted) and quinoline stacking

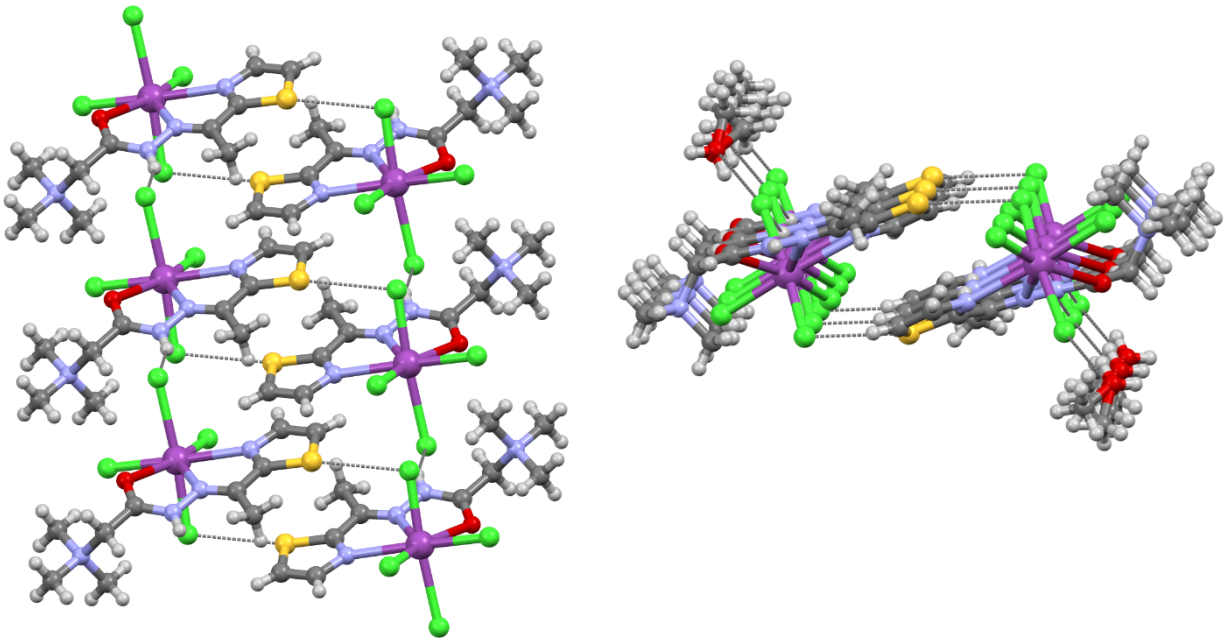

Fig. S2 Crystal packing of **2**, showing supramolecular ribbons held together by NH···Cl and Cl···S hydrogen and chalcogen bonds (left), decorated by hydrogen bonded solvation methanol molecules (right)

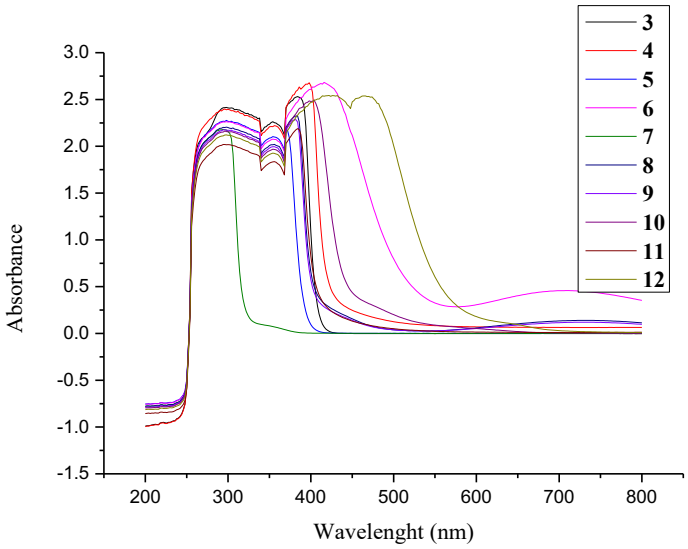

Fig. S3. UV–Vis absorption spectra of complex **3**–**12**

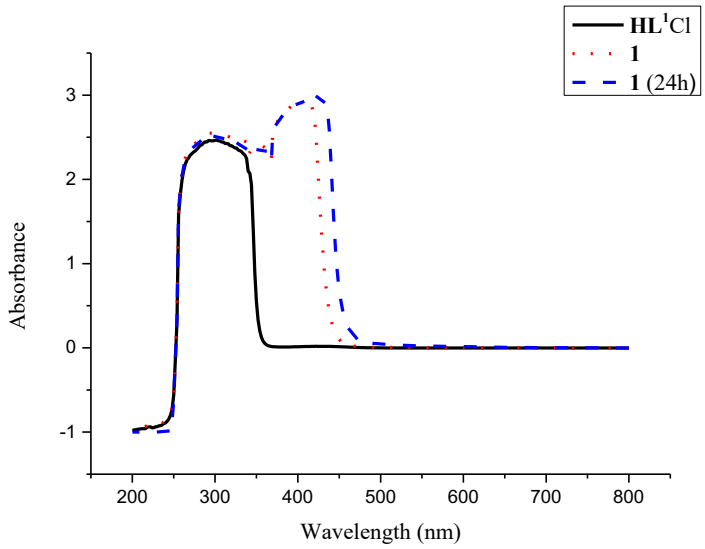

Fig. S4. UV–Vis absorption spectra of **HL**[1]Cl and complex **1**

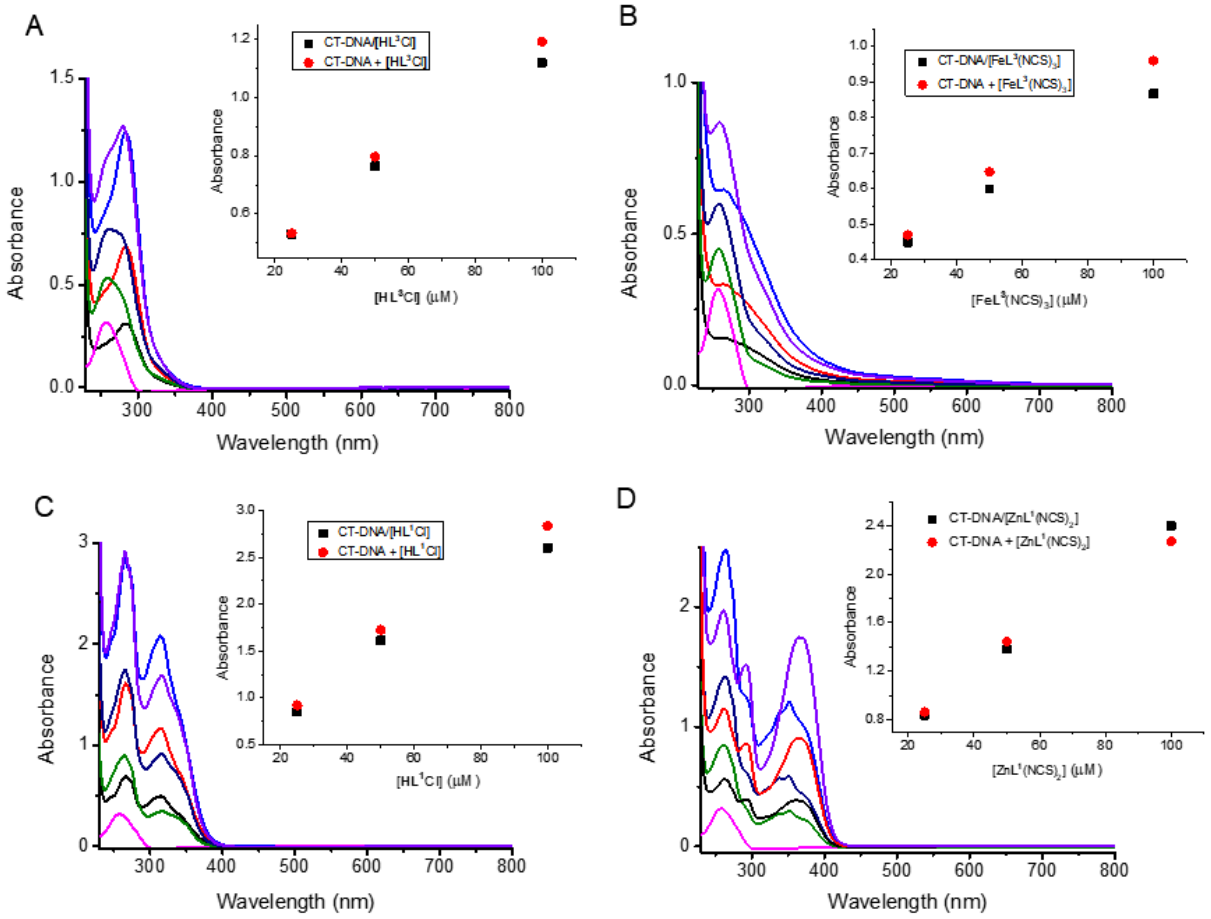

Fig. S5 Changes in UV–Vis absorption spectra of CT-DNA (48.5 μM) after interaction with different concentrations of the compounds: (a) **HL³**Cl (25, 50 and 100 μM); (b) **12** ([Fe**L³**(NCS)$_3$]) (25, 50 and 100 μM); (c) **HL¹**Cl (25, 50 and 100 μM) and (d) **1** ([Zn**L¹**(NCS)$_2$]) (25, 50 and 100 μM). In insets, comparison of absorbance at 258 nm between the CT-DNA–compound and the sum values of CT-DNA and compound

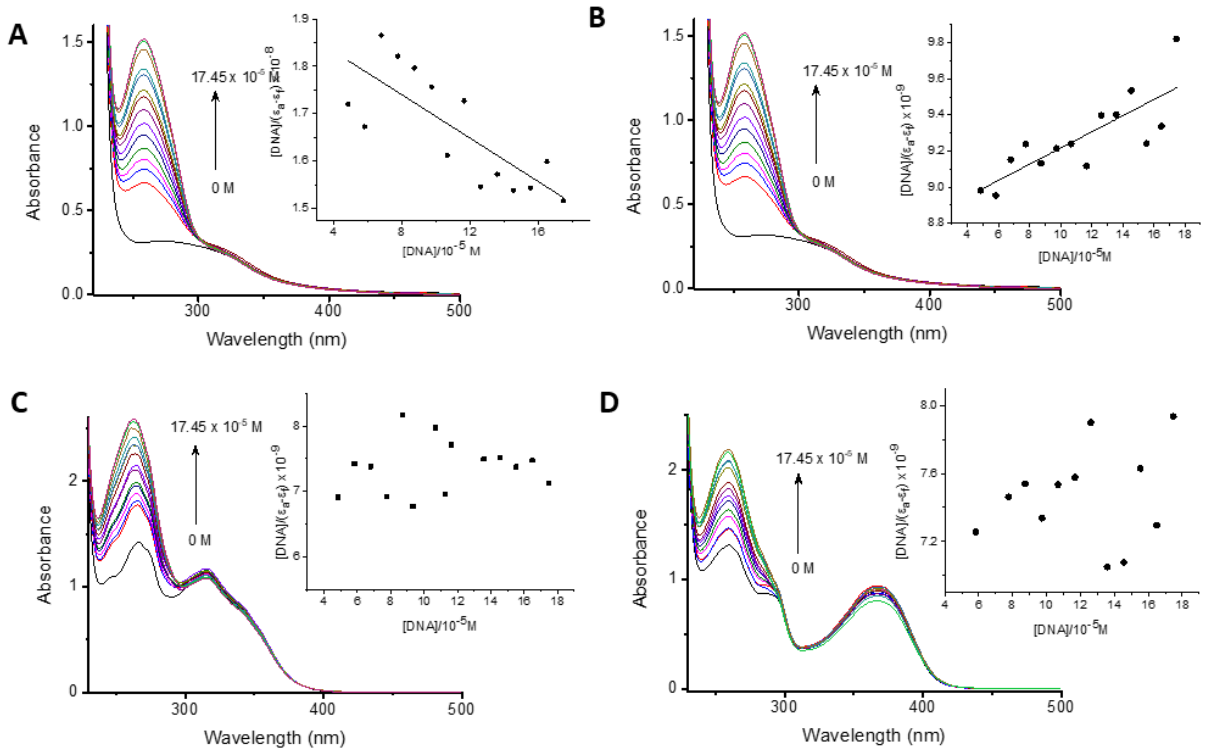

Fig. S6 UV−Vis absorption spectra of: (a)ligand **HL**^{3}Cl; (b)complex **12**; (c) ligand **HL**^{1}Cl and (d) complex **1** in the absence and presence of CT-DNA in 40 mM bicarbonate buffer (pH 8.0). Concentration of compounds was kept constant (50 μM) and concentrations of DNA varied ((4.85, 5.82, 6.79, 7.76, 8.73, 9.73, 10.67, 11.64, 12.61, 13,58, 14.55, 15.32, 16.49 and 17.46) x 10^{-5} M). The arrows show the changes in absorbance with increasing amounts of CT-DNA. Insets: plot of [DNA]/(ε_A – ε_F) *versus* [DNA]

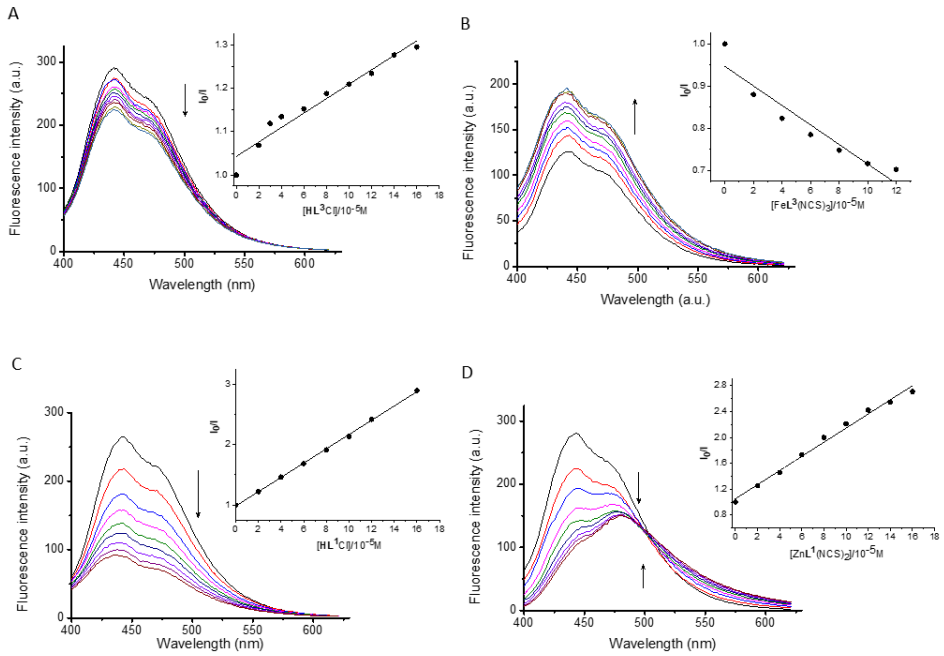

Fig. S7 Changes in emission spectra of Hoechst 33258 (2.5×10^{-5}M) bound to CT-DNA (9.7×10^{-5}M) by (a) ligand **HL^3**Cl, (b) complex **12** ([Fe**L^3**$(NCS)_3$]), (c) ligand **HL^1**Cl and (d) complex **1** ([Zn**L^1**$(NCS)_2$]) at increasing concentrations (2, 4, 6, 8, 10, 12, 14, 16, 18 $\times10^{-5}$ M). The arrows show that fluorescence intensity either decreased or increased with increasing concentration of the compound. The insets show fluorescence quenching curves of H bound to DNA at λ_{max}=441 nm by (a) **HL^3**Cl, (b) **12** ([Fe**L^3**$(NCS)_3$]), (c) **HL^1**Cl and (d) **1** ([Zn**L^1**$(NCS)_2$]). The quenching constant K_{sv} were calculated using Eq(2) by linear regression of a plot I_0/I against [Q], where I_0 and I represent the fluorescence intensities of H−CT-DNA in absence and presence of the compound, respectively, K_{sv} is the quenching constant and [Q] is the concentration ratio of the compound to DNA ([compound]/[CT-DNA]

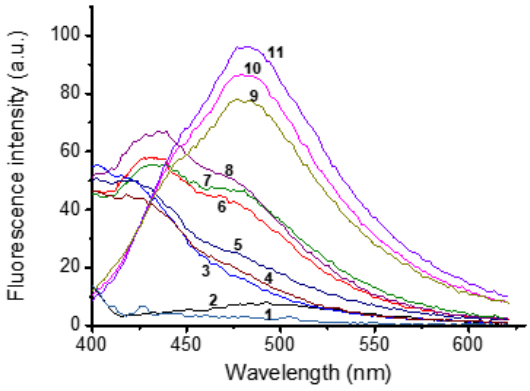

Fig. S8 Fluoresence spectra of H (2.5×10^{-5}M, curve 2); **HL^3**Cl (1×10^{-4}M, curve 1); **HL^1**Cl (1×10^{-4}M, curve 3); **HL^1**Cl−CT-DNA (1×10^{-4}M, curve 4); **HL^1**Cl−H (1×10^{-4}M, curve 5); **12** (1×10^{-4}M, curve 6); **12**−H (1×10^{-4}M, curve 7); **12**−CT-DNA (1×10^{-4}M, curve 8); **1**−CT-DNA (1×10^{-4}M, curve 9); **1** ($1x10^{-4}$M, curve 10); **1**−H (1×10^{-4}M, curve 11)

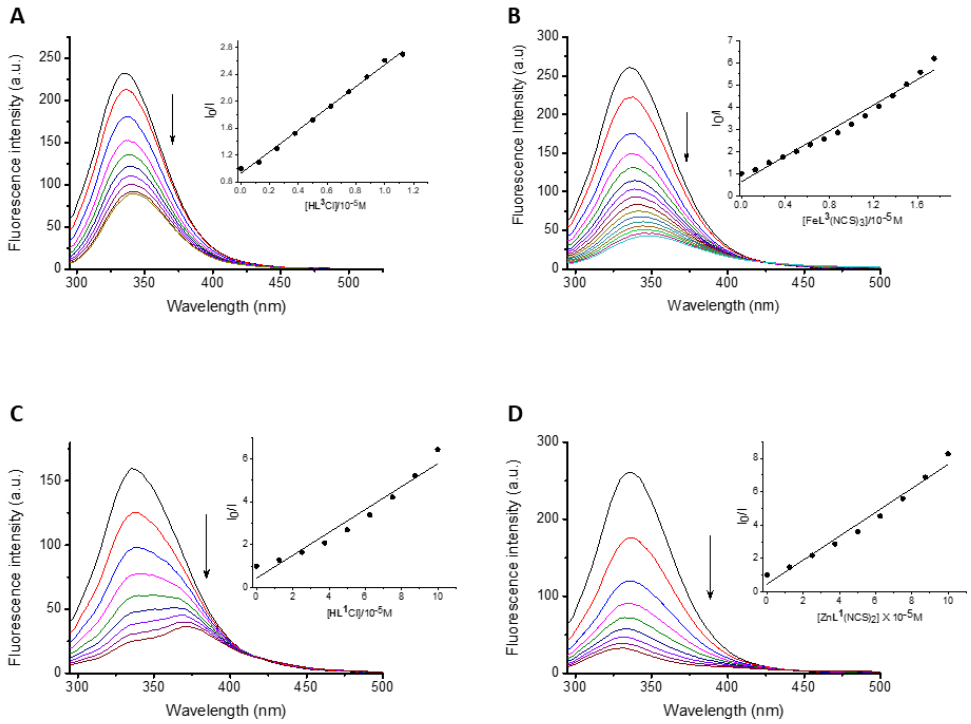

Fig. S9 Fluorescence spectra of BSA in the absence and presence of increasing concentrations of **HL^3**Cl, **12** ([Fe**L^3**(NCS)$_3$]), **HL^1**Cl and **1** ([Zn**L^1**(NCS)$_2$]) (a, b, c and d, respectively). Values of K_{sv} were calculated from the plot I_0/I versus [compound] shown in insets. The arrows show the decrease in fluorescence intensities with increasing concentrations of the compounds.

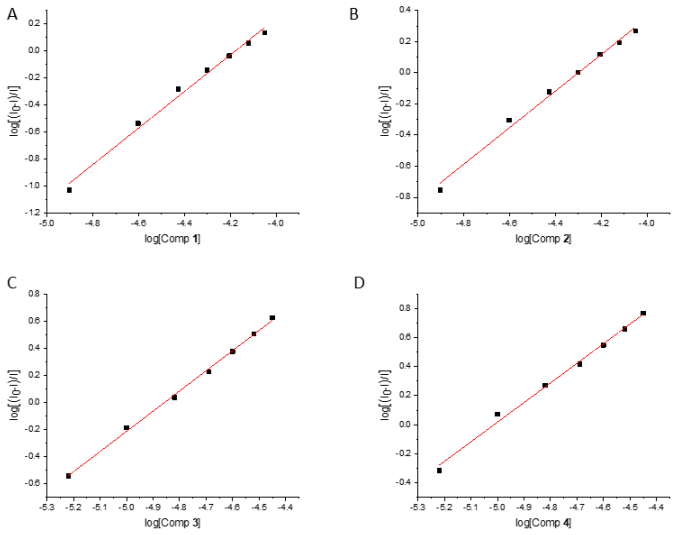

Fig. S10 Determination of K_b values for (a) **HL^3**Cl, (b) **12**, (c) **HL^1**Cl and (d) **1**, from the plots of log $[(I_0 - I)/I]$ *versus* log [compound]

References

1. Čobeljić B, Pevec A, Stepanović S, et al (2018) Structural diversity of isothiocyanato Cd(II) and Zn(II) Girard's T hydrazone complexes in solution and solid state: effect of H-bonding on coordination number and supramolecular assembly of Cd(II) complex in solid state. Structural Chemistry 29:1797–1806. https://doi.org/10.1007/s11224-018-1155-8
2. Adejumo TT, Tzouras N v., Zorba LP, et al (2020) Synthesis, Characterization, Catalytic Activity, and DFT Calculations of Zn(II) Hydrazone Complexes. Molecules 25:4043–4060. https://doi.org/10.3390/molecules25184043
3. Keškić T, Jagličić Z, Pevec A, et al (2020) Synthesis, X-ray structures and magnetic properties of Ni(II) complexes of heteroaromatic hydrazone. Polyhedron 191:114802–114814. https://doi.org/10.1016/j.poly.2020.114802
4. Milenković MR, Papastavrou AT, Radanović D, et al (2019) Highly-efficient N-arylation of imidazole catalyzed by Cu(II) complexes with quaternary ammonium-functionalized 2-acetylpyridine acylhydrazone. Polyhedron 165:22–30. https://doi.org/10.1016/j.poly.2019.03.001
5. Keškić T, Čobeljić B, Gruden M, et al (2019) What Is the Nature of Interactions of BF_4^-, NO_3^-, and ClO_4^- to Cu(II) Complexes with Girard's T Hydrazine? When Can Binuclear Complexes Be Formed? Crystal Growth & Design 19:4810–4821. https://doi.org/10.1021/acs.cgd.9b00760
6. Čobeljić B, Turel I, Pevec A, et al (2018) Synthesis, structures and magnetic properties of octahedral Co(III) complexes of heteroaromatic hydrazones with tetraisothiocyanato Co(II) anions. Polyhedron 155:425–432. https://doi.org/10.1016/j.poly.2018.08.070
7. Keskic T, Radanovic D, Pevec A, et al (2020) Synthesis, X-ray structure and DFT calculation of magnetic properties of binuclear Ni(II) complex with tridentate hydrazone-based ligand. Journal of the Serbian Chemical Society 85:1279–1290. https://doi.org/10.2298/JSC200625038K
8. Cobeljic B, Pevec A, Jaglicic Z, et al (2018) Synthesis, characterization and antimicrobial activity of isothiocyanato Fe(III) Girard's t hydrazone complex. Journal of the Serbian Chemical Society 83:1327–1337. https://doi.org/10.2298/JSC180828079C
9. Blois MS (1958) Antioxidant Determinations by the Use of a Stable Free Radical. Nature 181:1199–1200. https://doi.org/10.1038/1811199a0
10. Labieniec M, Gabryelak T (2006) Interactions of tannic acid and its derivatives (ellagic and gallic acid) with calf thymus DNA and bovine serum albumin using spectroscopic method. Journal of Photochemistry and Photobiology B: Biology 82:72–78. https://doi.org/10.1016/j.jphotobiol.2005.09.005

11. Ghosh K, Rathi S, Arora D (2016) Fluorescence spectral studies on interaction of fluorescent probes with Bovine Serum Albumin (BSA). Journal of Luminescence 175:135–140. https://doi.org/10.1016/j.jlumin.2016.01.029
12. Banerjee P, Pramanik S, Sarkar A, Bhattacharya SC (2009) Deciphering the Fluorescence Resonance Energy Transfer Signature of 3-Pyrazolyl 2-Pyrazoline in Transport Proteinous Environment. The Journal of Physical Chemistry B 113:11429–11436. https://doi.org/10.1021/jp811479r